Received: 23 March 2023 | Revised: 13 August 2023 | Accepted: 24 August 2023

DOI: 10.1002/jrs.6606

RESEARCH ARTICLE

Journal of RAMAN SPECTROSCOPY WILEY

DNA i-motif formation at physiological pH revealed by Raman spectroscopy

Jan Palacký[1] | **Petra Školáková**[1] | **Daniel Renčiuk**[1] | **Peter Mojzeš**[2] | **Barbara Rossi**[3] | **Fatima Matroodi**[3] | **Michaela Vorlíčková**[1]

[1]Department of Biophysics of Nucleic Acids, Institute of Biophysics of the Czech Academy of Sciences, Brno, Czech Republic

[2]Institute of Physics, Faculty of Mathematics and Physics, Charles University, Prague 2, Czech Republic

[3]Elettra Sincrotrone Trieste S.C.p.A., Trieste, Italy

Correspondence
Michaela Vorlíčková and Jan Palacký, Department of Biophysics of Nucleic Acids, Institute of Biophysics of the Czech Academy of Sciences, Královopolská 135, Brno 612 65, Czech Republic.
Email: mifi@ibp.cz; janpalacky@ibp.cz

Funding information
SYMBIT, Grant/Award Numbers: KRF-2019R1A2C1003517, CZ.02.1.01/0.0/0.0/15_003/0000477; TRIL Program of the Abdus Salam International Centre for Theoretical Physics

Abstract

The intercalated motif (iM) is a four-stranded structure consisting of two parallel homoduplexes formed by hemiprotonated $C.C^+$ pairs and intercalated antiparallel to each other. iM is generally formed at acidic pH, as cytosine protonation is required for its formation. However, sequences with long cytosine tracts can form iM at physiological pH conditions. Here, we use both off-resonant Raman and UV-resonant Raman (using synchrotron radiation) spectroscopy (RS) to study the sequence $(C_9T_3)_3C_9$, which has been recently thoroughly analysed by other spectroscopic methods (CD, ^{1}H NMR). In line with these methods, RS has shown that $(C_9T_3)_3C_9$ adopts iM at neutral pH and the iM forms with slow kinetics, melts in multiple steps and exhibits a large thermal hysteresis between the folding and refolding processes. The presence of isosbestic points in the temperature-dependent Raman spectra (in line with the SVD analysis indicating just two independent spectral components) suggests that the $(C_9T_3)_3C_9$ is found as a mixture of disordered and ordered structures, the proportion of which is temperature dependent. The ordered iM species are believed to be composed of the same type of $C.C^+$ pairs but differing in their number and arrangement along the cytosine tracts. The related sequence $(C_9A_3)_3C_9$ shows the same behaviour as $(C_9T_3)_3C_9$, indicating that the substitution of adenine bases for thymine bases has little effect.

KEYWORDS

cytosine i-motif DNA, pH, Raman spectroscopy, singular value decomposition, UV-resonant Raman

1 | INTRODUCTION

DNA is a conformationally flexible molecule known to adopt a plethora of secondary structures such as different families (A, B and Z) of double helical conformations, parallel duplexes, triplexes, hairpins, guanine quadruplexes (G4) and cytosine tetraplexes also known as intercalated motifs or i-motifs.[1] The i-motif structure (hereafter abbreviated as iM), which is formed by C-rich sequences under acidic conditions, was first reported by

Gehring et al.[2] using NMR spectroscopy in 1993. The iM consists of two parallel homoduplexes bound by hemiprotonated $C.C^+$ pairs, which are mutually intercalated antiparallel to each other.[3] The iM forms more readily at acidic pH because cytosine protonation is critical for its formation. The optimum pH is near the pK_a for N3 in cytosine at ~4.8,[4] which has long led to speculation whether iM also exists under in vivo conditions. However, the biological relevance of iM is strongly supported by several recent studies suggesting iM formation in vivo.[5–8] Moreover, there is evidence that iM is stabilized at neutral pH under molecular crowding conditions[9,10] or in the presence of small-molecule ligands.[11] On the other hand, various cations such as sodium and ammonium can destabilize iM.[12,13] Intramolecular iMs are of particular interest because they can be found, for example, at telomeres[14,15] and in the promoter regions of many genes, where they can serve as binding sites for numerous transcription factors.[5,16–20] Knowledge of the balance between the formation of duplexes, iM and G-quadruplexes could be used to wisely design small ligands that regulate gene expression by modifying/stabilizing the relevant noncanonical structure.[4,21–24] By increasing the length of cytosine sequences (C_n), the iM formation is shifted to a nearly neutral pH.[15,19,25–27] We have recently shown[28] that the $(C_nT_3)_3C_n$ type DNA sequences form iMs at neutral pH already for $n > 3$. With increasing n, the iM structure usually tends to be more stable, the kinetics of its formation slows down and hysteresis between iM folding and refolding increases. For $n > 6$, the iM sequences melt in two or more separate steps,[19,26,28] indicating the presence of multiple structural species. We have shown that iM formation follows a kinetic partitioning mechanism (see Figure S1): At low temperatures, iMs form with fast kinetics. These mostly randomly paired iM species are kinetically trapped unless the temperature is raised. At higher temperatures, this imperfectly paired iM species melt and can be substituted by slower forming but better ordered iM structures. These species differ in thermostability and melt separately with increasing temperature. The need to melt the previously formed shorter iM blocks and refold the longer ones leads to the multiphasic shape of the melting curve.

In addition to the methods mentioned above, Raman spectroscopy (RS) can be used to study the DNA base pairing, including iMs, with the potential to distinguish various local structural aspects. RS has been widely used to characterize nucleic acids and their complexes with small molecule ligands, metal ions, proteins, among others, in solution.[29] While G-quadruplexes have been intensively studied in solution by RS (in the Thomas laboratory,[30–35] by us[36,37] and others[38,39]) as well as by UV-resonant Raman spectroscopy (UVRRS),[40–46] there is only one RS study of iMs by Benevides et al.[47] (identifying Raman markers connected with iM formation), and one UVRRS study by Amato et al.[48] (investigating pH-dependent transitions between iM and hairpin structures derived from the C-rich strand sequences of the *BCL2* and *KRAS* oncogenes). In the present work, RS and UVRRS spectroscopies are used to probe the iM structures of $(C_9T_3)_3C_9$ (hereinafter C9T3) and its 'adenine' variant $(C_9A_3)_3C_9$ (hereinafter C9A3) in solution. The long C-rich sequences were chosen as a model since they slowly adopt iMs, allowing them to be easily monitored by RS and the kinetics of their individual iM species to be resolved. The two sequences C9T3 and C9A3 are investigated to determine the effect of the non-cytosine bases, which are not involved in stabilizing the iM core and yet are expected to have distinct Raman spectral signatures. As in our earlier work, in which we demonstrated the use of RS to study different G-quadruplex arrangements of the human telomeric sequence $AG_3(TTAG_3)_3$),[37] we would like to present here basic methodological points for the study of iMs, which can serve as a starting point for their further investigation. Particularly, we want to contribute to the understanding of the properties of iM using the method reflecting distinct aspects in the DNA structure than traditional methods (CD, UV-absorption, ^{1}H NMR) and to see whether RS can identify some differences in individual iM structures.

2 | MATERIAL AND METHODS

2.1 | Samples

Two lyophilized and desalted DNA oligonucleotides, $(C_9T_3)_3C_9$ and $(C_9A_3)_3C_9$, referred to as C9T3 and C9A3 throughout the paper, were purchased from Sigma-Aldrich and used without further purification for all spectroscopic experiments. Their length homogeneity was verified by denaturing electrophoresis (20% acrylamide gel with 7 M urea running at 50°C for 1 h at the power output of 25 W in 1 × TBE buffer). Stock solutions of the oligonucleotides at a concentration of about 20 mM in nucleosides were prepared in deionized Milli-Q water (18 MΩ-cm, 25°C) using centrifugal filter devices (Amicon Ultra 3 K, Millipore) to remove traces of small molecules and/or countercations potentially present in the lyophilizate. Precise nucleoside concentrations were determined from the absorbance at 260 nm recorded with a Specord 250 plus UV/vis spectrophotometer (Analytik Jena, Germany) in 1 mM sodium phosphate buffer, 0.3 mM EDTA, pH 8.0 at temperature above 90°C and the extinction coefficients 7,617 and 8,370 M^{-1} cm^{-1} for

C9T3 and C9A3, respectively, calculated as described in Kejnovska et al.[49] All experiments were performed in 1× Britton-Robinson buffer, prepared from 40 mM H_3BO_3, 40 mM H_3PO_4, 40 mM CH_3COOH and 75 mM KOH for pH 8 (denoted hereafter as 1 × K-RB). Depending on the specific measurement, the samples were transferred into 1 × K-RB, pH 8.0, and pH was adjusted to pH 6.6 and 5.0, respectively, using 2 M HCl without further addition of salt. All reagents used for sample preparation were of analytical grade and obtained from Sigma-Aldrich. The DNA nucleoside concentrations used for off-resonant Raman, resonant Raman and CD experiments were 10, 1 and 1 mM, respectively. The oligonucleotide samples were denatured at high temperature (>90°C) and then cooled to a selected lower temperature before each experiment.

2.2 | Off-resonant Raman measurements

The off-resonant Raman measurements were conducted in the 90° scattering geometry on a homemade Raman instrument with a Jobin Yvon–Spex 270 M multi-channel monochromator (Horiba; 1,200 grooves per millimetre used) connected to a liquid nitrogen-cooled CCD detector (Princeton Instruments). All Raman spectra were acquired with a 532 nm excitation line generated by a continuous-wave solid-state Nd:YVO_4 laser (Verdi 2, Coherent) by means of frequency doubling. The laser beam power applied to the DNA samples was about 400 mW to avoid photodegradation and to obtain Raman spectra with a satisfactory signal-to-noise ratio within a reasonable acquisition time (0.5–2 min depending on the experiment). A holographic notch filter (532 nm, Kaiser) was put in front of the spectrometer slit to eliminate Rayleigh scattering. Raman measurements were performed in hermetically sealed demountable quartz microcells (approximately 4 μl in volume placed in a thermally insulated holder whose temperature could be controlled from 0°C to 100°C in 0.1°C steps; the estimated accuracy is approximately ±0.5°C). The measurements of the individual spectra within the temperature dependence took 8 min, of which 2 min were used for the actual collection of the spectra, and the remaining 6 min were reserved for the temperature change (temperature increase/decrease by 2°C) and for equilibration of the sample at the new temperature. A temperature step of 2°C in 8 min was chosen to match the previous UV-absorption measurement conditions (0.25°C/min) as closely as possible.[28] The wavenumber scale of each Raman spectrum was accurately calibrated using the emission spectrum of a neon glow lamp, which was acquired during the intermediate period when the temperature was changing. The estimated short-term stability of our calibration procedure was better than 0.1 cm^{-1}. The spectrum collection time was 0.5 and 1 min for isothermal kinetic Raman measurements at 28°C and 42°C, respectively, and the neon calibration spectra could only be collected at their start and end. The processing of the raw Raman spectra was performed in a similar way as in the previous works.[36,37] The whole procedure of Raman spectra processing used in this paper is shown graphically in Figure S2 (and described in detail in the corresponding figure caption). First, the Raman spectra of the buffer were subtracted from the corresponding (i.e., taken at the same temperature and pH) raw Raman spectra. Next, relatively small contribution of non-Raman spectral background was suppressed by using previously described singular value decomposition (SVD)-based approach.[50] The background-corrected spectra were finally normalized to the 1,093 cm^{-1} peak, which has long been described as insensitive to DNA duplex melting.[51] The spectral region 850–1,150 cm^{-1} was excluded from further analysis and interpretation since it contains only very weak DNA bands (with the exception of the phosphate peak at ∼1,093 cm^{-1} used for intensity normalization), but, on the contrary, it contains relatively strong bands of buffer (877, 928, 990 and 1,078 cm^{-1}) whose positions and intensities depend on pH (see Figure S3) and which cannot be completely removed even after careful buffer subtraction.

2.3 | Ultraviolet resonant Raman measurements

Resonant Raman measurements were carried out at BL10.2-IUVS beamline of Elettra Sincrotrone Trieste (Italy)[52] using two excitation wavelengths 226 and 250 nm provided by the emission of the synchrotron radiation (SR) source. The exciting energies were selected by setting the suitable aperture gap of the undulator and using a Czerny-Turner monochromator (Acton SP2750, Princeton Instruments) equipped with 3,600 and 1,800 grooves per millimetre gratings to monochromatize the incoming SR. UVRRS spectra were collected in Suprasil® quartz cuvettes (placed in a thermally insulated holder, thermal stability ±0.1°C) using the backscattering configuration with a Czerny-Turner spectrometer (TriVista 557, Princeton Instruments, focal length 750 mm, holographic grating 1,800 grooves per millimetre) and a UV-optimized CCD camera, which provided a spectral resolution of approximately 15 cm^{-1}. The radiation power at the sample was only about 15 and 50 μW for the 226 and 250 nm excitation, respectively, meaning that, despite the resonance enhancement, each Raman

spectrum had to be collected for at least 30 min (usually three consecutive 10-min acquisitions) to achieve a satisfactory signal-to-noise ratio. Consequently, all UVRRS temperature-dependent spectra were measured with a much coarser step of 7°C than the corresponding off-resonant Raman spectra (step of 2°C). The spectrum collection time for isothermal kinetic Raman measurements was 15 min (still much longer than 0.5–1 min for off-resonant RS). To minimize possible photodegradation caused by prolonged exposure of DNA samples to UV light, the sample container was continuously oscillating along a single axis perpendicular to Raman excitation beam during the measurements. The damaging effect of UV radiation was estimated by measuring the CD spectra of the oligonucleotide samples before and after Raman measurements, and only minor photodegradation was detected for the samples prepared at near-neutral pH. The calibration of wavenumber scale was performed using cyclohexane (spectroscopic grade, Sigma-Aldrich). Basic processing of raw UVRRS spectra including the elimination of cosmic rays and merging consecutive spectral acquisitions into one spectrum was performed in TriVista software (Princeton Instruments) and LabSpec 6 (Horiba Scientific). The solvent contribution could not be simply subtracted from the UVRRS spectra due to the well-known self-absorption effect (residing in the nonlinearity of the UVRRS intensities with the concentration of sample components), the correction of which is impractical for our purposes, as it needs precise knowledge of many sampling parameters, such as the optical path and the sampling geometry.[53–55] Thus, our UVRRS spectra may contain spectral traces of buffer (which, however, is expected to be negligible in the spectral range of interest when using UV excitation) as well as the prominent water deformation band at ~1,640 cm^{-1} (which is, however, largely independent of temperature[50] and the concentrations of solutes). In addition, our UVRRS spectra measured in quartz cuvettes were not corrected for the parasitic spectral contribution of the quartz, which has major bands at ~790, 1,060 and 1,200 cm^{-1}.[56] The spectra were normalized to integral intensity in the fingerprint region (rather than to a particular band) due to the unknown/complex wavenumber dependence of reabsorption.

2.4 | CD measurements

The CD spectra were recorded using a Jasco J815 spectrometer (Tokyo, Japan). Each CD spectrum was measured at a scan rate of 100 nm/min with a data spacing of 0.5 nm and corresponded to the average of four scans. CD magnitude was expressed as the molar absorption difference of left- and right-circularly polarized light (with molarity being related to DNA strand concentration). For the measurement of CD spectra at high DNA nucleoside concentration (~10 mM), it was necessary to use thin sealable quartz cuvettes with a pathlength of 0.1 mm. The temperature in the cuvette was controlled within a range of 1°C by inserting it into the thermostatic cuvette holder.

2.5 | SVD analysis

The spectral changes taking place as a function of a given physicochemical parameter (temperature, time, etc.) can be most simply visualized by plotting the selected spectral intensities versus that parameter for selected independent variables (wavelength, wavenumbers, etc.). Such univariate curves are easy to interpret but can be sensitive to noise, even when constructed from smoothed data. All spectral changes can be also depicted simultaneously (i.e., considering the entire spectral range) using a multivariate approach based on SVD decomposition,[50] according to which the original spectrum $\boldsymbol{Y_i}$ within a particular dataset can alternatively be expressed as $Y_i = \sum_j W_j V_{ij} U_j$, where the sum represents a finite linear combination of the orthonormal basis spectra $\boldsymbol{U_j}$ weighted by the singular values W_j (sorted by convention in descending order) with the coefficients V_{ij} representing the contribution of the basis spectrum $\boldsymbol{U_j}$ to the spectrum $\boldsymbol{Y_i}$. The above summation can be restricted to j less than or equal to some threshold value j_{max}, where the components $\boldsymbol{U_j}$ for $j > j_{max}$ (with comparatively small singular values W_j) add primarily noise to the reconstructed spectra, highlighting the advantage of the SVD approach to filter out noise from the raw data. The threshold value j_{max} corresponding to the dimensionality of the data (the so-called factor dimension) can be estimated from a plot of the singular values against their respective order j as the value at which the singular values stop decreasing significantly and their decline follows a linear trend.[57] The SVD analyses applied to the temperature dependencies and time evolutions of Raman spectra presented in this work have factor dimension 3 at most, which facilitates their interpretation. Particularly, the first orthonormal component $\boldsymbol{U_1}$ is like the average spectrum, as it represents the best description of each dataset spectrum using just one orthonormal spectral component. The values of the corresponding coefficient $\boldsymbol{V_1}$ (its component V_{i1} represents the intensity of the ith spectrum) are roughly constant for the datasets in this paper due to spectra normalization to the phosphate peak at 1,093 cm^{-1}. The second orthonormal component $\boldsymbol{U_2}$ is more informative, as it describes the major spectral changes not accounted for by the

component U_1. The values of the corresponding coefficient V_2 plotted as a function of the parameter assigned to each spectrum (temperature, time, etc.) typically strongly resemble conventional univariate curves (such as melting curves), but unlike them, they are not as noisy, which makes their interpretation much clearer. The SVD results in this work include not only the plots of singular values but also the plots of explained variances (expressed in %), where the explained variance associated with a given orthonormal component is calculated as the ratio of the square of the corresponding singular value divided by the sum of the squares of all singular values. SVD analyses and all auxiliary calculations are performed in the Python 3 programming language, mainly using the powerful NumPy library.

3 | RESULTS AND DISCUSSION

3.1 | The effect of pH

The Raman spectra of C9T3 at pH 5.0, 6.6 and 8.0 measured at ambient temperature (23°C) are shown in Figure 1. As evident from their difference, the spectra at pH 5.0 and 6.6 are very similar, indicating that C9T3 does not undergo any notable structural change between those two pHs. Interestingly, however, the Raman spectrum at pH 6.6 shows a Raman peak at 1,529 cm^{-1}, which is not present in the otherwise similar Raman spectrum at pH 5 but can be found in the Raman spectrum at pH 8. Furthermore, these Raman spectra are similar to the spectra

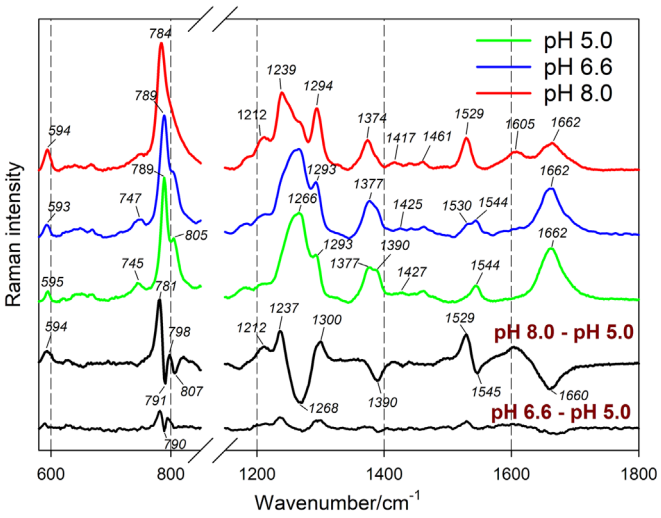

FIGURE 1 Raman spectra of $(C_9T_3)_3C_9$ at 23°C and pH 5.0 (green line), pH 6.6 (blue line) and pH 8.0 (red line). The spectra at the bottom correspond to the difference between the spectrum recorded at pH 6.6 (bottommost), pH 8.0 and the spectrum at pH 5.0. The nucleoside concentration is 10 mM.

previously reported by Benevides et al.[47] for C_3T and C_8, which form iMs at acidic pH. A fundamental question arises as to whether the Raman spectra at low pH reflect merely the hemiprotonation at N3, which may be concerted or not with iM formation, or whether there are also Raman bands associated exclusively with iM formation. Interestingly, Benevides et al. proposed that the band at ~806 cm^{-1} (assigned to phosphate backbone stretch incorporating C3′-endo nucleosides) can be considered an iM marker.[47] Consistently, our Raman spectra at acidic pH contain the band around 805 cm^{-1} (close to and overlapping with the much more intensive band around 789 cm^{-1} assigned to pyrimidine bases[29]), which disappears at pH 8.0 (see Figure 1). The CD spectrum of C9T3, measured under the same buffer conditions (pH 6.6) and at the same nucleoside concentration (10 mM) as the corresponding Raman spectrum, is also consistent with the presence of iM, as evidenced by the positive CD band at ~287 nm (see Figure S4). While C9T3 at pH 6.6 retains its iM structure, a further increase in pH to 8.0 leads to large spectral changes that can be interpreted as a destabilization of iM (see Figure 1), consistent with all previous studies suggesting that even iMs composed of lengthy C-rich sequences cannot withstand such a high alkaline pH.[8,12,15,19,26,27,58,59] The CD spectrum of C9T3 measured under the same buffer conditions (pH 8.0) and at the same nucleoside concentration (10 mM) as the corresponding Raman spectrum confirms the disruption of iM at high alkaline pH, as evidenced by the disappearance of the negative CD band at ~265 nm and the downshift (to ~278 nm) and decrease of the positive band at ~287 nm (see Figure S4). The difference Raman spectrum between pH 8.0 and pH 5.0 shows the distinctive spectral changes with increasing pH (see Figure 1), which involve a frequency downshift of the highest band at ~789 cm^{-1} (roughly 5 cm^{-1}), a decrease in intensity at ~805, ~1,268, ~1,390, ~1,545 and ~1,660 cm^{-1} and an increase in intensity at ~1,212, ~1,237, 1,294 and 1,529 cm^{-1}. This difference spectrum has virtually the same shape as that of C_3T and C_8 described by Benevides et al.[47] The Raman spectra of C9A3 show the same pattern of pH spectral changes as those of C9T3 (compare Figures 1 and S5) and can be interpreted in the same way. The formation of iM at a slightly less acidic pH (6.6) is again confirmed by CD spectroscopy (see Figure S4).

3.2 | Thermal denaturation/renaturation

Increasing temperature has the same impact on the iM structure as increasing pH, as indicated by the striking

similarity of the Raman spectral changes observed in the melting/annealing Raman experiment with C9T3 at pH 6.6 to those presented in the previous section (cf. the difference spectrum in Figure 1 and in the upper left part of Figure 2). Univariate thermal curves constructed by plotting the Raman intensity versus temperature at selected wavenumbers exhibit a multiphasic character (best represented probably by the 1,270 cm^{-1} univariate dependence and the coefficient $\boldsymbol{V_2}$ from the SVD analysis; for details, see Figure 2 and the corresponding figure caption) and a hysteresis between the melting and annealing process, in full agreement with our and other data obtained by other spectroscopic methods.[19,26,27] The multiphasic shape of the Raman melting curves can be linked to the presence of multiple i-motif conformations with distinct thermal stabilities. The temperature-dependent Raman spectra of C9T3 are linearly dependent because each of them can be approximated very well as a linear combination of two pure spectra, one corresponding to a fully thermostable i-motif at the lowest measured temperature (2°C) and the other to a temperature-denatured structure at the highest measured temperature (see Figure 3). This is in line with the corresponding SVD analysis indicating the factor dimension close to 2 (see Figure S6), the presence of isosbestic points in the temperature-dependent spectra of C9T3 (see the Raman spectra in the lower left part of Figure 2) and the same spectral shape and positions of the isosbestic points for the melting and cooling directions of C9T3 as well as C9A3 (see Figure S7). The plot of the decomposition coefficients in Figure 3 also nicely reflects the multiphasic nature of the thermal iM denaturation.

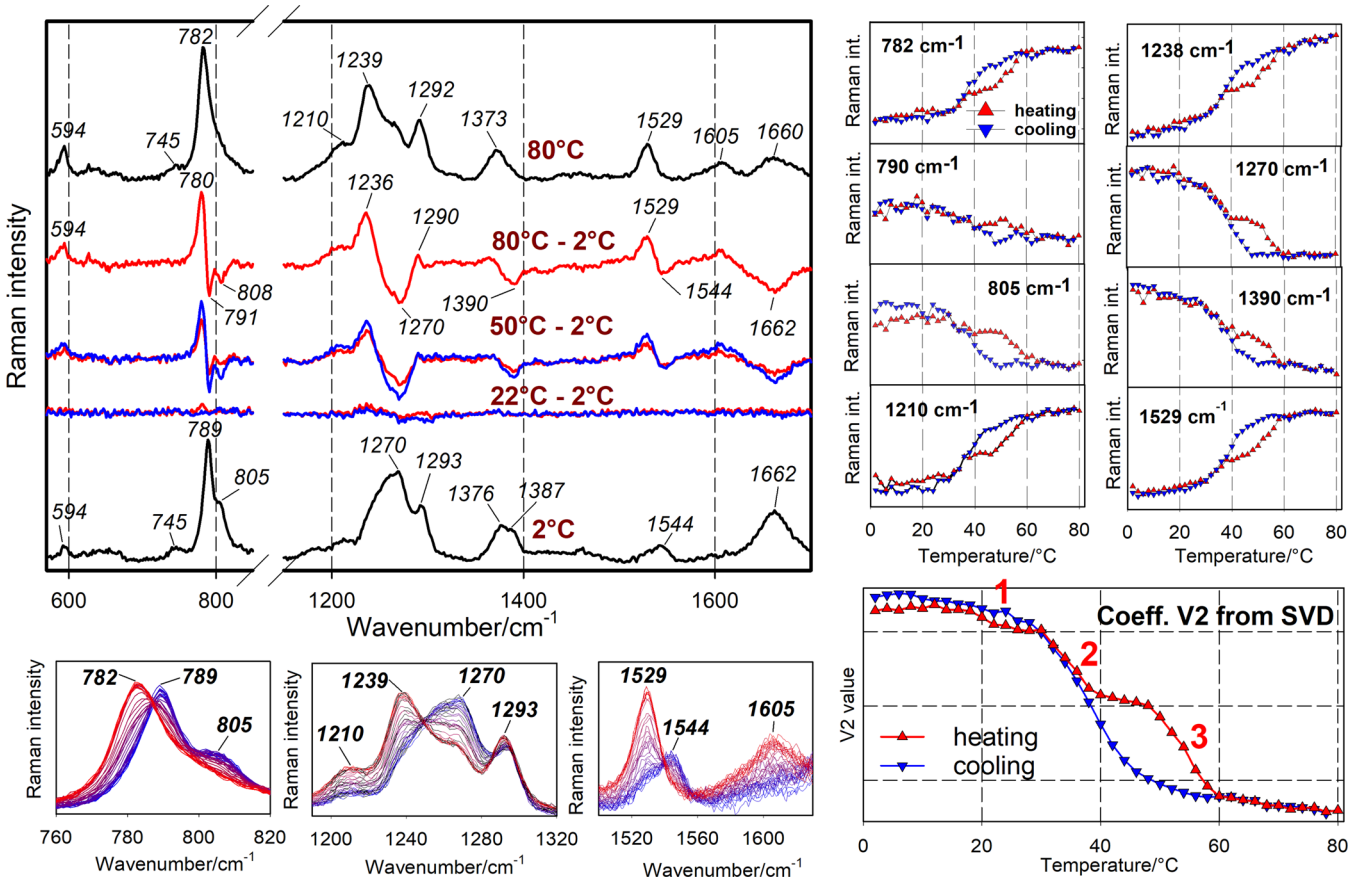

FIGURE 2 Temperature-dependent Raman spectra of $(C_9T_3)_3C_9$ at pH 6.6. The nucleoside concentration is 10 mM. Upper left: Thermal transition between the Raman spectrum of $(C_9T_3)_3C_9$ at 2°C (the bottommost) and 80°C (topmost). The spectra in between the spectrum at 2°C and 80°C correspond (in order from the bottom) to the difference between the spectrum at 22°C, 50°C, 80°C and the spectrum at 2°C. The difference spectra in red (blue) correspond to the heating (cooling) direction. Bottom left: Raman spectra for the heating direction plotted using a gradient palette between blue (2°C) and red (80°C) shown in three spectral regions. Upper right: intensities at the selected wavenumbers of the smoothed (using the Savitzky–Golay filter with window length = 25 and polynomial order = 2) Raman spectra of $(C_9T_3)_3C_9$ at pH 6.6 plotted as a function of temperature for the melting (red points) and cooling (blue points) direction. Bottom right: the coefficient $\boldsymbol{V_2}$ (see Section 2.5) from SVD analysis of the Raman spectra of $(C_9T_3)_3C_9$ at pH 6.6 for the melting (red line with red points) and cooling (blue line with blue points) direction. The melting curve shows multiple thermal transitions (at least three) and significant hysteresis between the melting and cooling curves.

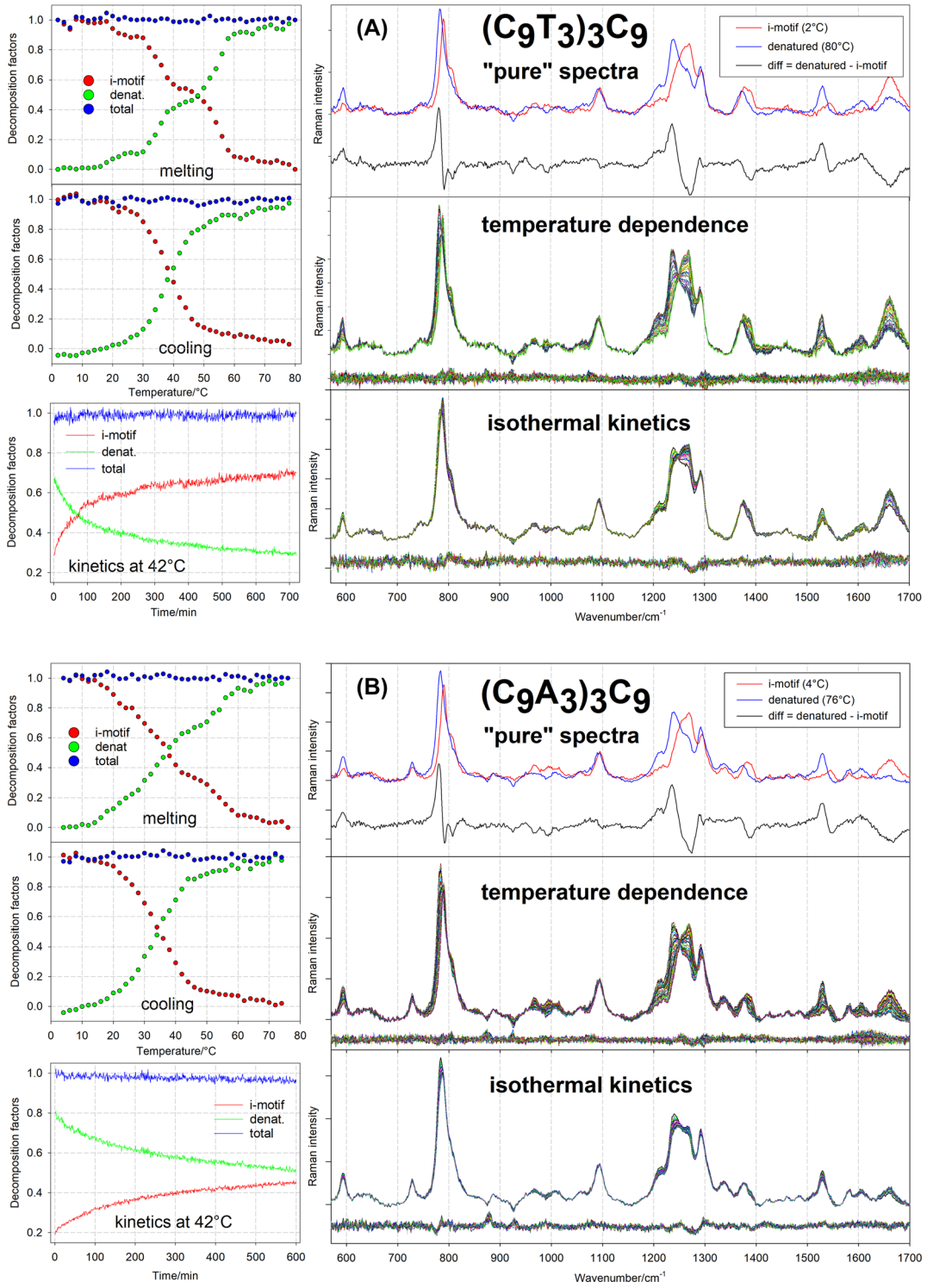

FIGURE 3 Legend on next page.

FIGURE 3 Top part of the figure (part A): decomposition of the Raman spectra of $(C_9T_3)_3C_9$ at pH 6.6 into the Raman spectrum of its structured (i-motif) and unfolded (denatured) form. Uppermost right plot of part A ('pure spectra'): the Raman spectrum of $(C_9T_3)_3C_9$ at 2°C (red line; predominately i-motif), at 80°C (blue line; predominately unstructured form) and the corresponding difference Raman spectrum between the Raman spectrum of the unstructured and the i-motif form (black line). Middle right (temperature dependence) and bottommost right (isothermal kinetics) plots of part A: artificial Raman spectra constructed using appropriate linear combinations of the pure spectra shown in the uppermost right plot of part A, such that each artificial spectrum is as close as possible (in the least squares sense) to the original spectrum at a given temperature in the case of temperature-dependent spectra (middle right) or at a given time in the case of isothermal (at 42°C) time-dependent Raman spectra (bottommost right). In both cases, all residual spectra between the reconstructed and original Raman spectra are shown to estimate the accuracy of the fit. Left plots of part A: the decomposition coefficients are shown as a function of temperature for the temperature-dependent Raman spectra (for the melting and cooling direction separately) and as a function of time for the isothermal (at 42°C) time-dependent Raman spectra. Decomposition coefficients corresponding to the i-motif and the denatured form are plotted in red and green (points for thermal experiments and lines for kinetic experiments). The sum of the decomposition coefficients for the two forms into which the decomposition is performed is shown in blue (it is expected to be around 1). Bottom part of the figure (part B): decomposition of the Raman spectra of $(C_9A_3)_3C_9$ at pH 6.6 into the Raman spectrum of its structured (i-motif) and unfolded (denatured) form. Uppermost right plot of part B ("pure spectra"): the Raman spectrum of $(C_9A_3)_3C_9$ at 4°C (red line; predominately i-motif), at 76°C (blue line; predominately unstructured form) and the corresponding difference Raman spectrum between the Raman spectrum of the unstructured and the i-motif form (black line). Middle right (temperature dependence) and bottommost right (isothermal kinetics) plots of part B and left plots of part B: the same description as for the corresponding part of the figure (A).

The same thermal experiment as with C9T3 performed with C9A3 shows that substitution of thymines for adenines in the iM loops does not alter the overall character and interpretation of the temperature-dependent spectral changes (cf. Figure 2 with Figure S8). The main difference between the Raman spectra of C9T3 and C9A3 is, as expected, the presence of ring mode bands, which are exclusive to thymine (at ~745 cm^{-1}) or adenine (at ~728, ~1,337 and ~1,580 cm^{-1}) bases.[29] Interestingly, these 'pure' A or T Raman bands are relatively insensitive to both pH and temperature change, indicating that the iM structures of C9T3 and C9A3 are predominantly determined by $C.C^+$ pairs. The thermal hysteresis is also observed in C9A3, but it is less pronounced, and the melting transitions are less evident than in C9T3 (cf. the $\boldsymbol{V_2}$ plot from the SVD analysis shown in the lower right part of Figures 2 and S8). Again, as in the case of C9T3, the temperature-dependent Raman spectra of C9A3 are linearly dependent and can be expressed roughly as a linear combination of two spectra, corresponding to the ordered iM form and the denatured structure (see Figure 3). Accordingly, the corresponding SVD analysis again points to the factor dimension close to 2 (the statistical weights of the higher orthonormal components $\boldsymbol{U_j}$, $j > 2$, are substantially smaller; see Figure S6). The positions of the isosbestic points for the melting and cooling directions of C9A3 are the same and very similar to those of C9T3 (see Figure S7).

Thermal melting and annealing experiments were also performed using SR with 250 nm as excitation wavelength, which, due to resonance enhancement, allowed us to obtain Raman spectra at relatively low nucleoside concentrations (~1 mM), i.e., 10 times lower than those used in the off-resonant Raman measurements. The results of UVRRS temperature-dependent measurements done with C9T3 at pH 5.0, pH 6.6 and pH 8.0 are summarized in Figure 4. In contrast to off-resonant Raman spectra, the UVRRS spectra have much broader bands (spectral resolution ~15 cm^{-1}), are noisier, less spectrally rich, and do not change appreciably with temperature, except for the bands at ~1,530, ~1,480 (only at pH 8.0), and 1,650 cm^{-1}. The nicely resolved UVRRS band at ~1,530 cm^{-1}, which is resonantly enhanced throughout the deep UV region, is assigned to cytosine (being the most prominent spectral feature in the UVRRS spectra) and is related to its ring mode that involves N3-C4 bond stretching.[60–62] The 1,530 cm^{-1} band is found at all pHs and increases with increasing temperature, which is the same behaviour as observed for the off-resonant Raman spectra (see Figure 2), where it is connected with thermal destabilization of the iM structure. An analogous increase in the intensity of the 1,530 cm^{-1} cytosine band was observed during the thermal denaturation of DNA hairpin and duplex structures.[63] This cytosine band also increases in intensity during the pH-induced denaturation of dC_{12} as documented by IR spectroscopy.[64] Despite the temperature step of 7°C for the UVRRS melting/cooling measurements being larger compared to the step of 2°C for the off-resonant RS measurements (since each UVRRS spectrum had to be accumulated for a longer time, i.e., 30 min), some qualitative conclusions can still be drawn from the temperature-dependent UVRRS spectra. The melting/annealing curves that follow the UVRRS intensity at 1,530 cm^{-1} with the corresponding spectra for the melting direction are shown for each experiment in Figure 4. The smallest spectral change of the 1,530 cm^{-1} band is observed at pH 5.0, where its

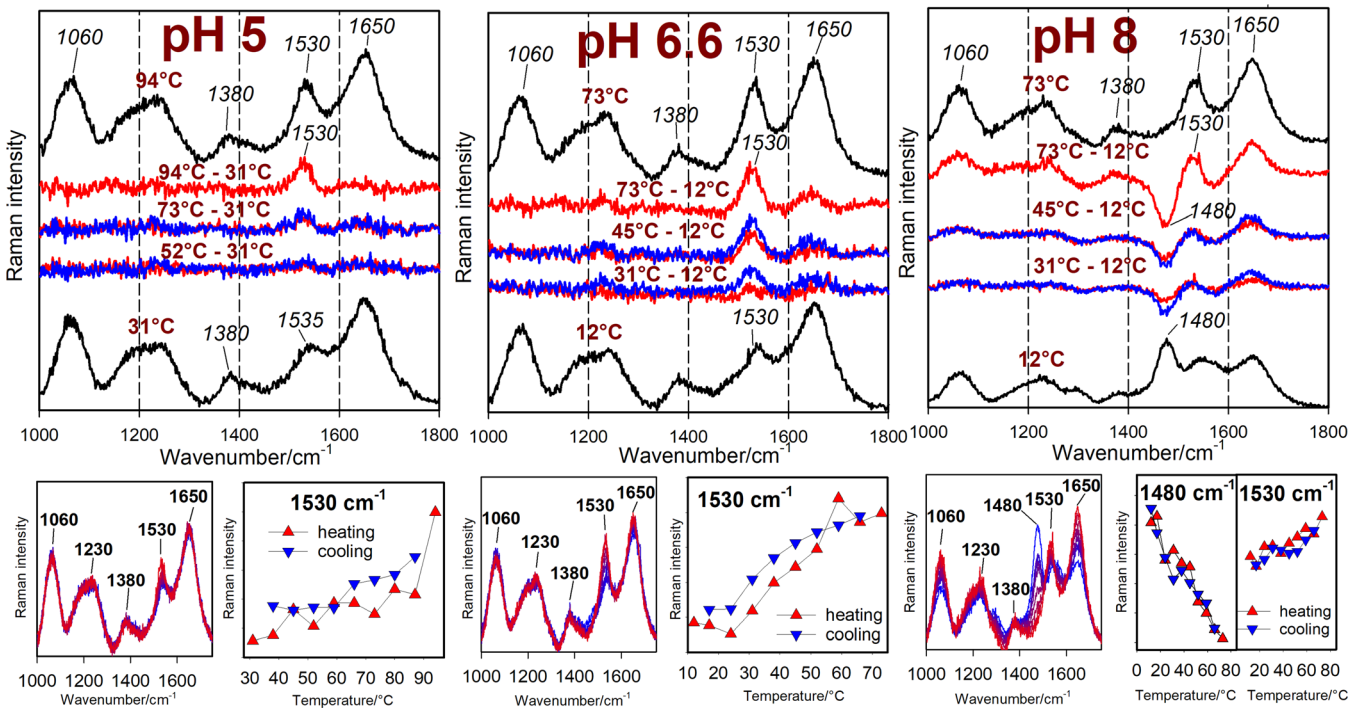

FIGURE 4 Temperature-dependent UVRRS spectra (excitation 250 nm) of $(C_9T_3)_3C_9$ recorded at pH 5.0 (left), pH 6.6 (middle) and pH 8.0 (right). The nucleoside concentration is 1 mM. Upper left (pH 5): thermal transition between the UVRRS spectrum of $(C_9T_3)_3C_9$ at 31°C (the bottommost) and 94°C (topmost). The spectra in between correspond (in order from the bottom) to the difference between the spectrum at 52°C, 73°C, 94°C and the spectrum at 31°C. The difference spectra in red (blue) correspond to the heating (cooling) direction. Upper middle (pH 6.6) and upper right (pH 8.0): thermal transition between the UVRRS spectrum of $(C_9T_3)_3C_9$ at 12°C (bottommost) and 73°C (topmost). The spectra in between correspond (in order from the bottom) to the difference between the spectrum at 31°C, 45°C, 73°C and the spectrum at 12°C. The difference spectra in red (blue) correspond to the heating (cooling) direction. Bottom: Raman spectra for the heating direction plotted using a gradient palette between blue for the lowest temperature (31°C for pH 5.0 and 12°C for other pHs) and red for the highest temperature (94°C for pH 5.0 and 73°C for other pHs) together with melting (red points) and cooling curves (blue points) based on the Raman intensity at 1,530 cm^{-1} (and also at 1,480 cm^{-1} for pH 8.0) of the smoothed (using the Savitzky–Golay filter with window length = 25 and polynomial order = 2) Raman spectra plotted as a function of temperature.

intensity starts to increase significantly only at the highest temperatures (>80°C), which agrees with our previous UV-abs and differential scanning calorimetry (DSC) data indicating the thermostability of C9T3 at acidic pH 5.0 far above 80°C.[27] The largest spectral change of the 1,530 cm^{-1} band is observed at pH 6.6, where its intensity increases steadily above room temperature, while the slope of the change decreases at higher temperatures. In addition, there is an obvious hysteresis between the melting and annealing dependence of C9T3 at pH 6.6 (see the corresponding 1,530 cm^{-1} dependence and the difference spectra in the middle part of Figure 4). This is in quantitative agreement with our earlier UV-abs data (obtained under comparable experimental conditions to the UVRRS measurements), which show that the thermostability of C9T3 at pH 6.5 is roughly 50°C and that hysteresis is present.[27] The behaviour of the 1,530 cm^{-1} band at pH 8.0 is tricky to interpret since at pH 8.0, the iM structure of C9T3 is expected to be unfolded based on the UV absorption thermal melting and renaturation experiments at 297 nm (the wavelength reflecting iM formation[28]) at the same nucleoside concentration of 1 mM as that used for UVRR measurements (see Figure S9). We still see that the 1,530 cm^{-1} band increases with temperature, but this change is overshadowed by the larger spectral changes of the 1,480 and 1,650 cm^{-1} bands. The band at ~1,480 cm^{-1}, assigned to deoxyribonucleotides of adenine and thymine but not to cytosine,[60,62] has a peculiar behaviour. It appears that the intensity of the 1,480 cm^{-1} band of both C9T3 (see Figure 4) and C9A3 (see Figure S10) decreases with increasing temperature, as confirmed by repeated measurements, and its changes are observed particularly at basic pH (8.0). For unknown reasons, this band did not always behave predictably in our experiments (especially at lower temperatures), and its intensity sometimes changed rapidly from one value to another even for spectra measured at close temperatures. It is not clear why the

band at ~1,480 cm^{-1} is so sensitive to temperature changes under highly alkaline conditions (pH 8.0). This behaviour can be partly attributed to the increased sensitivity of the 1,480 cm^{-1} band to excessive UV radiation during long UVRRS experiments.[65] Finally, the UVRRS band at ~1,650 cm^{-1} (both cytosine and thymine contribute to this band[62]) tends to increase in intensity with temperature (at pH 6.6 and 8.0) for C9T3 (see Figure 4) and C9A3 (see Figure S10). Such a thermal hyperchromism was attributed to disruption of the ordered structure of DNA.[63] In addition to the bands described above, the only other bands found in the UVRRS spectra of C9T3 are around 1,060, 1,200 and 1,380 cm^{-1}, but these do not change with temperature. The main spectral contribution at ~1,060 and ~1,200 cm^{-1} likely comes from the spectrum of the glass cuvette.[56] The invariance of the band at ~1,380 cm^{-1} (attributed to combined ring stretching and C6-H in-plane deformation of thymine residues[62,66,67]) may imply that thymine loops do not play an essential role during thermal unfolding of iM, as this band has been described as an indicator of thymine environment or interaction.[29] The UVRRS spectral changes observed upon thermal denaturation of C9T3 are similar to those of C9A3 (cf. Figures 4 and S10), except that the thymine band at ~1,380 cm^{-1} in C9T3 is replaced by the adenine band at ~1,335 cm^{-1} in C9A3 (attributed to stretching vibrations of its C5-N7 and N7-C8 bonds[60]), which is also not very sensitive to temperature (see Figure S10).

3.3 | Isothermal kinetic experiments

At moderately high temperatures (~40°C) and at near-neutral pH, the formation of thermodynamically equilibrium iM structures takes a longer time (>10 h; depending on the exact pH and the exact temperature[28]), which allows more precise ordering of the alternating $C.C^+$ pairs; thus, the formation of longer blocks of consecutive $C.C^+$ pairs than in the case of the rapidly formed iMs at low temperatures. Our previous results indicate that the thermodynamic stability of iM is mostly determined by the number of consecutive regularly alternating intercalated parallel and antiparallel $C.C^+$ pairs, rather than by the total number of $C.C^+$ pairs in the structure.[15] Here, RS data follow the isothermal kinetics of C9T3 at pH 6.6 and 42°C starting from the denatured state at >90°C and recorded immediately after rapid cooling to 42°C (see Figure 5). This kinetics is slow enough to be captured by our Raman device (compared to the very fast kinetics at low temperature or at acidic pH). The time-dependent Raman spectra of C9T3 at 42°C (pH 6.6) reflecting the gradual increase in the amount of iM over time exhibit similar spectral changes (cf. Figures 1, 2 and 5) like those observed with decreasing temperature or decreasing pH. These spectra show a high degree of linear dependence, as evidenced by the fact that each spectrum from the time kinetics of C9T3 at 42°C can be expressed reasonably well as a linear combination of just two 'pure' Raman spectra (see Figure 3). These 'pure' Raman spectra are the same as those that have already been used for the spectral decomposition of temperature-dependent Raman spectra, as discussed in the previous section (i.e., the spectrum of the pure i-motif and the spectrum of the denatured form). This is in line with the corresponding SVD analysis, which implies the factor dimension close to 2 (see the left panel of Figure S11). The extent of spectral changes for the time-kinetic experiment is significantly smaller than for the temperature dependence (cf. Figures 2 and 5), which is partly due to the dead time (it takes approximately 5 min for the sample temperature to stabilize at 42°C, and therefore, the measurement starts when a certain amount of the iM structure has already formed) and partly because the relative amount of the equilibrium iM structure at 42°C is less than the maximum amount of the iM structure at the lowest temperature of 2°C. Specifically, from the time evolution of the decomposition coefficients for C9T3, it can be roughly estimated that approximately 29% of the iM structure is present at the beginning of the time kinetics measurement, while after 12 h the amount of iM structure increases and stabilizes at approximately 70% (see Figure 3). The same spectral decomposition can be successfully performed for C9A3, where the relative amount of iM structure at the beginning of the time kinetics measurement is approximately 19% and the saturated iM concentration is approximately 45% (see Figure 3). The smaller amount of iM in the saturation phase of the isothermal kinetics correlates nicely with the fact that C9A3 is slightly less thermostable than C9T3 under otherwise identical conditions (see the plot of the $\boldsymbol{V_2}$ coefficient vs temperature in Figure S6). Alternatively, this means that at a fixed temperature of 42°C, C9A3 is less folded than C9T3.

Interestingly, the time-dependent isothermal spectra of C9T3 at 42°C do not show the clear presence of isosbestic points (as in the temperature-dependent spectra shown in the lower left part of Figure 2), as one would expect in accordance with the proposed presence of two spectral forms (see the lower left part of Figure 5). While the 1,200–1,320 cm^{-1} and 1,500–1,630 cm^{-1} regions show hints of isosbestic points, there is no sign of isosbestic behaviour in the 760–820 cm^{-1} region (one can see that the pyrimidine ring stretch band shifts with time from ~784 to ~789 cm^{-1} without any noticeable change in intensity). The reason why the isosbestic points in the time-kinetic spectra are harder to detect

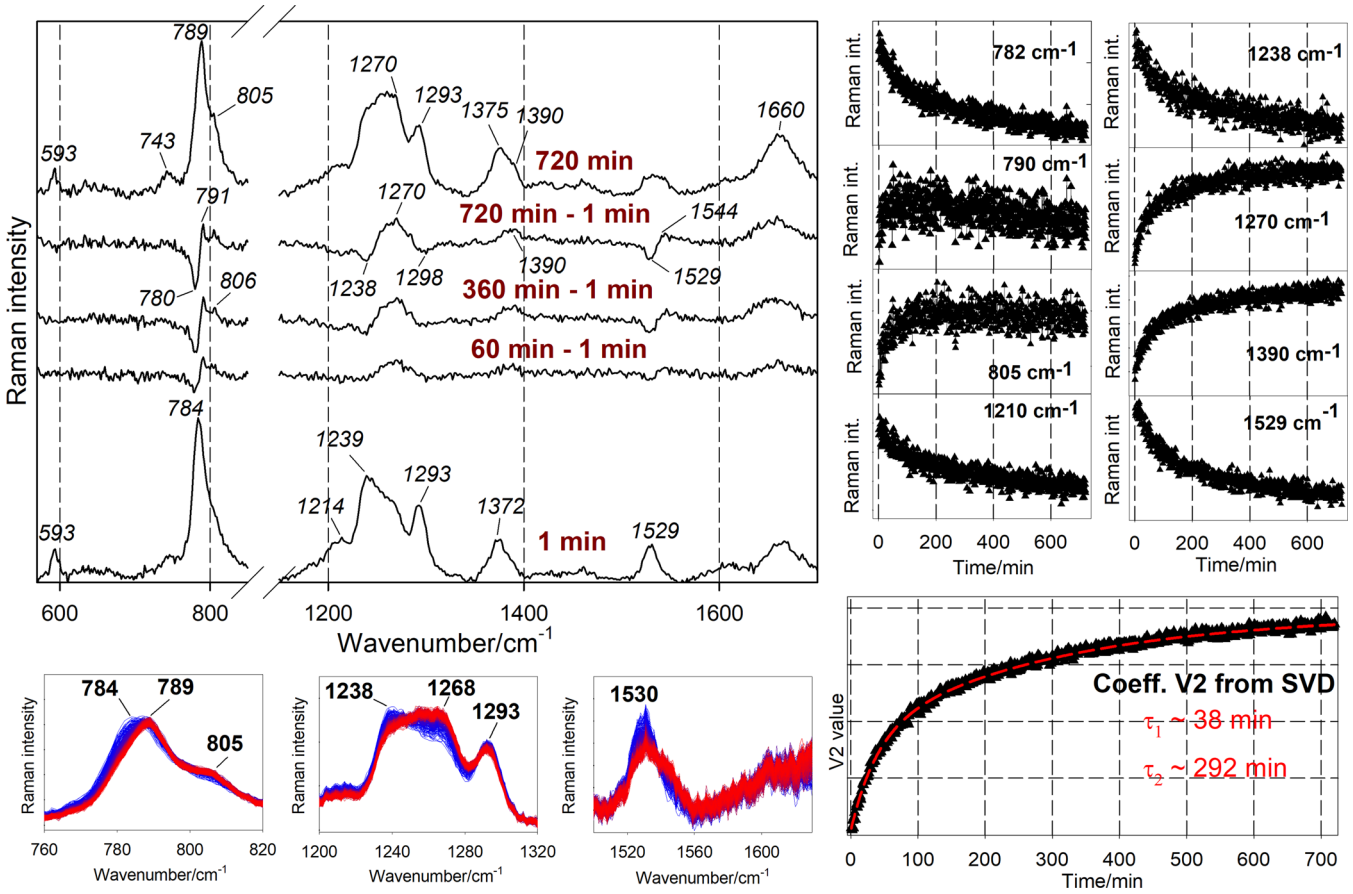

FIGURE 5 Time-dependent Raman spectra of $(C_9T_3)_3C_9$ at pH 6.6 recorded immediately after denaturation at high temperature and rapid cooling to 42°C. The nucleoside concentration is 10 mM. Upper left: time-dependent transition between the Raman spectrum of $(C_9T_3)_3C_9$ recorded at the onset of the isothermal kinetics at 42°C (bottommost) and after 720 min (topmost). The spectra in between the initial and final spectrum of the kinetics correspond (in order from the bottom) to the difference between the spectrum recorded at times 60 min, 360 min, 720 min and the initial spectrum. Bottom left: Raman spectra for the heating direction plotted using a gradient palette between blue (initial spectrum) and red (final spectrum) shown in three spectral regions. Upper right: intensities at the selected wavenumbers of the smoothed (using the Savitzky–Golay filter with window length = 25 and polynomial order = 2) time-dependent Raman spectra of $(C_9T_3)_3C_9$ at pH 6.6 plotted as a function of time for the melting (red points) and cooling (blue points) direction. Bottom right: isothermal kinetics at 42°C represented by the coefficient $\boldsymbol{V_2}$ from SVD analysis (see the text for details) against time. The slow (τ_1–38 min) and fast (τ_2–292 min) time constants are obtained by fitting the double exponential fit to the coefficient $\boldsymbol{V_2}$.

(if they exist at all) may be partly due to the smaller extent of spectral changes (as described above) and partly due to the slightly larger noise in the time-kinetic spectra compared to the temperature-dependent spectra (the collection time of the time-kinetic spectra of C9T3 was shorter [1 min] than the collection time of the temperature-dependent spectra [2 min]). The identification of isosbestic points may have been slightly affected by the pre-processing of the Raman spectra themselves, especially their intensity normalization (see Section 2 for details). For instance, it is tricky to explain why C9A3, which otherwise behaves very similarly to C9T3 in temperature-dependent (see Figure S6) and isothermal kinetics experiments (see Figure S11), exhibits a slightly varying intensity of the pyrimidine band at 785–788 cm^{-1} with time (see the lower left part of Figure S12). Hence, we are unable to verify beyond reasonable doubt the presence of isosbestic points (especially in the 760–820 cm^{-1} region). Their presence would mean that, in fact, there are many transient structures during the isothermal kinetic experiment. This interpretation is consistent with our understanding of the behaviour of long cytosine sequences such as C9T3. A rough estimate of the rate of spectral changes during isothermal kinetics at 42°C for C9T3 and C9A3 is obtained by fitting the double-exponential curve defined by $y_0 + a(1 - \exp(-t/\tau_1)) + b(1 - \exp(-t/\tau_2))$, where t is the time and y_0, a and b are the fitting parameters, to the $\boldsymbol{V_2}$ coefficient profile extracted from the SVD analysis of

the respective isothermal kinetics (see Figure S11). The double exponential fit is proper for both isothermal kinetics and the obtained time constants are similar for C9T3 ($\tau_1 = 38$ min, $\tau_2 = 292$ min) and C9A3 ($\tau_1 = 41$ min, $\tau_2 = 300$ min).

The isothermal kinetics for C9T3 at 42°C was also studied by UV-resonant RS using 226 and 250 nm excitations. The UVRRS experiments were performed under the same buffer conditions as the off-resonant Raman experiments, but at an order of magnitude lower concentration (~1 mM). The SVD analysis of the UVRRS data reveals subtle spectral changes that are not easily detectable by the naked eye (see Figure S13). Although the variability within the UVRRS spectra for both excitations is well explained by the first component $\boldsymbol{U_1}$ (resembling the average spectrum), as indicated by the factor dimension of the UVRRS data being close to 1 (see the plots of singular values at the bottom of Figure S13), the second orthonormal component $\boldsymbol{U_2}$, with a relatively small statistical weight still shows little spectral variation in the band at ~1,535 cm^{-1}. The corresponding coefficient $\boldsymbol{V_2}$ indicates that the intensity of the band at ~1,535 cm^{-1} decreases very slightly with temperature, which, as in the case of off-resonant Raman spectra, can be attributed to a gradual increase in the amount of iM with time.

3.4 | Isothermal kinetics versus thermal denaturation experiments

Figure 6 summarizes in a unified way the behaviour of C9T3 at near-neutral pH (6.6). This figure is based on more than 1,800 off-resonant Raman spectra combined from five experiments: (1) thermal denaturation/renaturation over the whole temperature range 0–80°C, (2) 'fast' isothermal kinetics at 28°C recorded for 1 h (after the temperature jump from >90°C), (3) thermal denaturation of the final iM formed at 28°C (recorded right from the moment when the 'fast' kinetics at 28°C is completed at equilibrium), (4) 'slow' isothermal kinetics at 42°C recorded for 12 h (after the temperature jump from >90°C) and (5) thermal denaturation of the final iM formed at 42°C (recorded right from the moment when the 'slow' kinetics at 42°C is completed at equilibrium). The U-profiles ($\boldsymbol{U_j}$, $j = 1, 2, 3$) located in the leftmost part of Figure 6 represent an orthonormal set of artificial spectra that can be combined to reconstruct the original data. The profile $\boldsymbol{U_1}$ most accurately describes (using only one orthonormal component) each original spectrum within the combined dataset and as such resembles an average spectrum. The profile $\boldsymbol{U_2}$ captures the most important spectral features common to all spectra in the combined

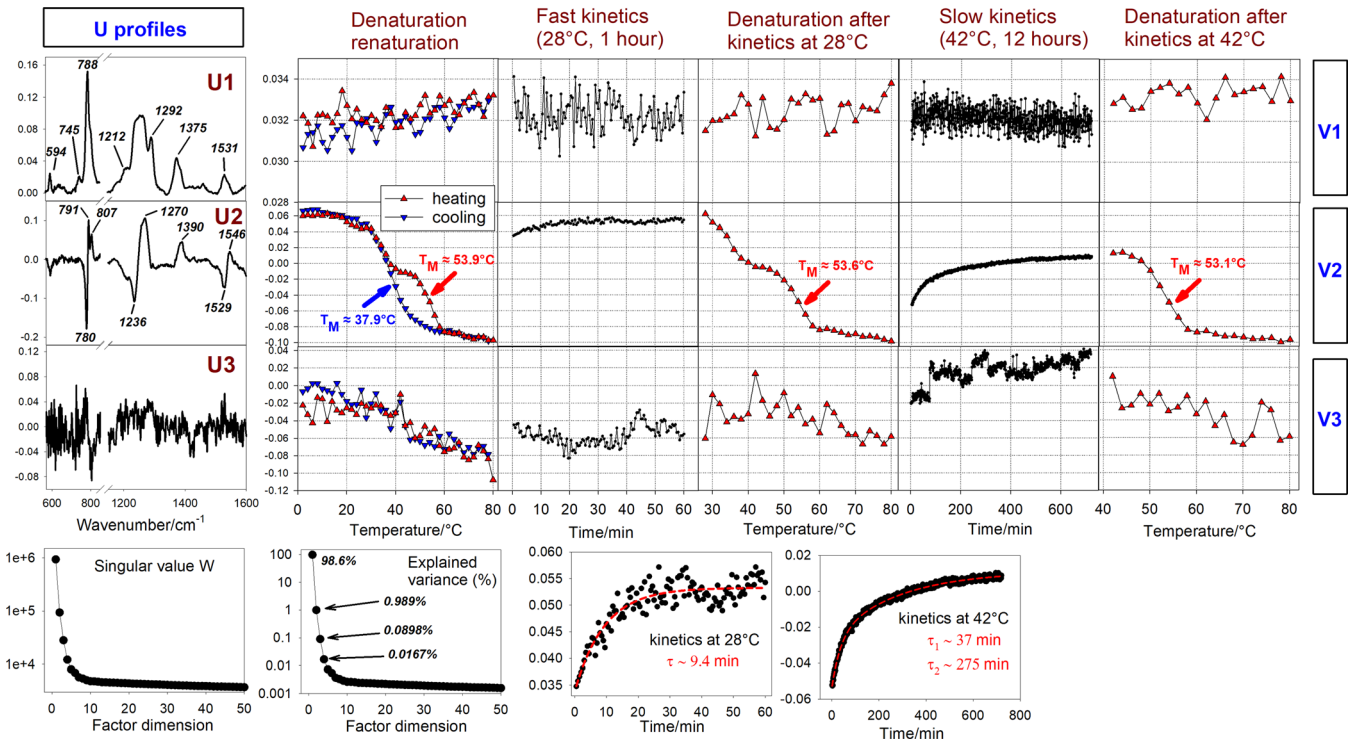

FIGURE 6 SVD analysis of a combined data set (from five experiments) of more than 1,800 off-resonant Raman spectra of $(C_9T_3)_3C_9$: denaturation/renaturation over the entire temperature range 0–80°C, fast kinetics at 28°C recorded for 1 h, thermal denaturation measured immediately after kinetics at 28°C, slow kinetics at 42°C recorded for 12 h and thermal denaturation measured immediately after kinetics at 42°C. A detailed explanation of this figure can be found in the last section of the article. The nucleoside concentration is 10 mM.

dataset. The spectral changes described by the profile U_2 are like the spectral changes accompanying the folding/refolding of iM structures, as can be seen by comparing the profile U_2 with the pH- and temperature-dependent difference spectra (see Figures 1 and 2) and the difference spectra for isothermal kinetics at 42°C (see Figure 5). Note that the spectral changes induced by increasing pH/temperature (by which the iM structure is gradually destabilized) proceed in the opposite direction to the changes occurring during the isothermal kinetics at 42°C (where the amount of iM structure gradually increases), as emphasized in the previous section. It was not easy to estimate the factor dimension in this case (it seemed to be four or more), but since the singular values corresponding to U_3 and U_4 were noticeably smaller than that for U_2 (3.3 and 7.7 times, respectively) and, importantly, U_3 and the higher order profiles U_j for $j > 3$ were contributing predominately to a stochastic noise, each spectrum of the combined dataset was possible to approximate (up to the noise level) by a linear combination of U_1 and U_2. The coefficients V_j, $j = 1, 2, 3$ represented by the rows to the right of the U-profiles (Figure 6) determine for each spectrum the relative contribution that the profiles U_j, $j = 1, 2, 3$ add to the resulting linear combination. The values of each coefficient V_j are split up into five columns, with each coefficient representing one experiment described above. The coefficient V_1 is mostly constant, since the spectral contribution of the 'average' profile U_1 to each original spectrum is ascribed mainly to its total spectral intensity, which does not vary much between spectra since all of them have been normalized to the phosphate peak at 1,093 cm^{-1}. More interesting is the behaviour of the coefficient V_2 (associated with the profile U_2 capturing the largest spectral variability, as mentioned above), whose shape resembles simple univariate curves (obtained by plotting the Raman intensity at selected wavenumbers), but unlike them, it is less sensitive to noise. The isothermal kinetics at 28°C is substantially faster than the kinetics at 42°C. It is so fast that the range of changes in V_2 values is noticeably smaller compared to the kinetics at 42°C, mainly because it takes some time to start the measurement after preparing the sample. Unlike the isothermal kinetics at 42°C, the isothermal kinetics at 28°C (represented by the coefficient V_2) can be fitted properly by using just the single-exponential fit defined by $y_0 + a(1 - \exp(-t/\tau))$, where t is the time and y_0 and a are the fitting parameters (the obtained time constant $\tau \approx 9$ min). Importantly, thermal denaturation starting from 2°C, 28°C and 42°C undergoes three, two or one melting steps, respectively, depending on which structures have already melted.[28] The transition temperature of the most stable iM phase is about the same (≈53–54°C) for all three denaturation experiments.

4 | CONCLUSIONS

Except for the pioneer work of Benevides et al.[47] from 1996, the utility of RS for structural studies of i-motifs has not been tested at all. The aim of this paper is to fill this methodological gap. We demonstrate here the applicability of RS for the characterization of the model C-rich DNA sequences, which have been thoroughly studied and described in our very recent work using other experimental techniques, primarily CD and NMR spectroscopy.[28] We specifically deal with the sequences $(C_9T_3)_3C_9$ and $(C_9A_3)_3C_9$, which, due to their long cytosine runs, adopt iM structure at pH close to neutral. As the process of iM formation and disintegration is relatively slow, its kinetics can be readily monitored by RS. We have identified characteristic Raman features reflecting protonation state of cytosine, iM formation, and confirmed that it proceeds via a complex partitioning mechanism. At low temperatures, the iMs consisting of short randomly paired $C.C^+$ blocks, formed rapidly. At slightly sub-physiological temperatures (here 28°C), these not fully ordered iM structures were melting away and were replaced by slower forming but more thermostable structures containing longer blocks of consecutive $C.C^+$ pairs until eventually a fully and perfectly ordered iM structure was formed (here at 42°C).

The key finding and contribution of the present work are an unambiguous demonstration that the Raman spectra of individual iM structures are linearly dependent. The temperature dependence and isothermal time kinetics of the Raman spectra of both C9T3 and C9A3 suggest the presence of two spectral/structural components that reflect a variable amount of ordered and disordered DNA structures as a function of temperature and time. Thus, according to RS, individual iM structures differ only in the extent of their ordered and disordered forms, that is, in the length of uninterrupted blocks of consecutive $C.C^+$ pairs. Apart from the expected differences due to the Raman contribution of adenine and thymine residues in the loops, Raman spectra of C9T3 and C9A3 do not show any significant differences, suggesting that the nature of the bases in loops has a little effect on the structure of iMs and the mechanism of their formation. The conclusions arising from UV resonant RS (UVRRS) at one order of magnitude lower nucleotide concentration are qualitatively consistent with those from the off-resonant RS. As there is still inconsistency in opinions on the biological relevance of iMs formation under physiological conditions where high concentration and molecular crowding may play an important role, the capability of RS and UVRRS to extend the concentration range of iMs studies beyond the range accessible by UV-abs and CD spectroscopies

can be useful. Similarly, the complex nature of Raman spectra providing information on the iMs parts as well as loops can be considered as a methodological advantage. The RS and UVRRS are thus potentially valuable methods for studies where conventional spectroscopic methods are not applicable.

ACKNOWLEDGEMENTS

This work was supported by the project SYMBIT reg. number: CZ.02.1.01/0.0/0.0/15_003/0000477. We acknowledge Elettra Sincrotrone Trieste for providing access to its synchrotron radiation facilities and for financial support under the IUS internal project. FM gratefully acknowledges funding by TRIL Program of the Abdus Salam International Centre for Theoretical Physics (ICTP).

ORCID

Jan Palacký https://orcid.org/0000-0002-8603-9103
Petra Školáková https://orcid.org/0000-0002-0072-7010
Daniel Renčiuk https://orcid.org/0000-0001-9293-7105
Peter Mojzeš https://orcid.org/0000-0002-9952-6939
Barbara Rossi https://orcid.org/0000-0003-1357-8074
Fatima Matroodi https://orcid.org/0000-0002-0989-0463
Michaela Vorlíčková https://orcid.org/0000-0002-9153-5099

REFERENCES

[1] A. Bansal, S. Kaushik, S. Kukreti, *Front. Genet.* **2022**, *13*, 959258.
[2] K. Gehring, J. L. Leroy, M. Gueron, *Nature* **1993**, *363*, 561.
[3] M. Gueron, J. L. Leroy, *Curr. Opin. Struct. Biol.* **2000**, *10*, 326.
[4] S. S. Masoud, K. Nagasawa, *Chem. Pharm. Bull.* **2018**, *66*, 1091.
[5] M. Zeraati, D. B. Langley, P. Schofield, A. L. Moye, R. Rouet, W. E. Hughes, T. M. Bryan, M. E. Dinger, D. Christ, *Nat. Chem.* **2018**, *10*, 631.
[6] S. Dzatko, M. Krafcikova, R. Hansel-Hertsch, T. Fessl, R. Fiala, T. Loja, D. Krafcik, J. L. Mergny, S. Foldynova-Trantirkova, L. Trantirek, *Angew. Chem. Int. Ed.* **2018**, *57*, 2165.
[7] W. H. Tang, K. K. Niu, G. X. Yu, Y. Jin, X. Zhang, Y. L. Peng, S. N. Chen, H. M. Deng, S. Li, J. Wang, Q. S. Song, Q. L. Feng, *Epigenetics Chromatin* **2020**, *13*, 12.
[8] M. P. Cheng, D. H. Qiu, L. Tamon, E. Istvankova, P. Viskova, S. Amrane, A. Guedin, J. L. Chen, L. Lacroix, H. X. Ju, L. Trantirek, A. B. Sahakyan, J. Zhou, J. L. Mergny, *Angew. Chem. Int. Ed.* **2021**, *60*, 10286.
[9] A. Rajendran, S. Nakano, N. Sugimoto, *Chem. Commun.* **2010**, *46*, 1299.
[10] Y. P. Bhaysar-Jog, E. van Dornshuld, T. A. Brooks, G. S. Tschumper, R. M. Wadkins, *Biochemistry* **2014**, *53*, 1586.
[11] E. P. Wright, H. A. Day, A. M. Ibrahim, J. Kumar, L. J. E. Boswell, C. Huguin, C. E. M. Stevenson, K. Pors, Z. A. E. Waller, *Sci. Rep.* **2016**, *6*, 7.
[12] J. L. Mergny, L. Lacroix, X. G. Han, J. L. Leroy, C. Helene, *J. Am. Chem. Soc.* **1995**, *117*, 8887.
[13] N. Iaccarino, A. di Porzio, J. Amato, B. Pagano, D. Brancaccio, E. Novellino, R. Leardi, A. Randazzo, *Anal. Bioanal. Chem.* **2019**, *411*, 7473.
[14] S. Fernandez, R. Eritja, A. Avino, J. Jaumot, R. Gargallo, *Int. J. Biol. Macromol.* **2011**, *49*, 729.
[15] Z. Dvořáková, D. Renčiuk, I. Kejnovská, P. Školáková, K. Bednářová, J. Sagi, M. Vorlíčková, *Nucleic Acids Res.* **2018**, *46*, 1624.
[16] J. A. Brazier, A. Shah, G. D. Brown, *Chem. Commun.* **2012**, *48*, 10739.
[17] S. Dhakal, Z. B. Yu, R. Konik, Y. X. Cui, D. Koirala, H. B. Mao, *Biophys. J.* **2012**, *102*, 2575.
[18] Y. X. Cui, D. M. Kong, C. Ghimire, C. X. Xu, H. B. Mao, *Biochem.* **2016**, *55*, 2291.
[19] E. P. Wright, J. L. Huppert, Z. A. E. Waller, *Nucleic Acids Res.* **2017**, *45*, 2951.
[20] K. L. Irving, J. J. King, Z. A. E. Waller, C. W. Evans, N. M. Smith, *Biochimie* **2022**, *198*, 33.
[21] M. del Toro, P. Bucek, A. Avino, J. Jaumot, C. Gonzalez, R. Eritja, R. Gargallo, *Biochimie* **2009**, *91*, 894.
[22] H. A. Day, P. Pavlou, Z. A. E. Waller, *Bioorg. Med. Chem.* **2014**, *22*, 4407.
[23] J. J. King, K. L. Irving, C. W. Evans, R. V. Chikhale, R. Becker, C. J. Morris, C. D. P. Martinez, P. Schofield, D. Christ, L. H. Hurley, Z. A. E. Waller, K. S. Iyer, N. M. Smith, *J. Am. Chem. Soc.* **2020**, *142*, 20600.
[24] S. L. Brown, S. Kendrick, *Pharmaceuticals* **2021**, *14*, 24.
[25] G. Manzini, N. Yathindra, L. E. Xodo, *Nucleic Acids Res.* **1994**, *22*, 4634.
[26] R. A. Rogers, A. M. Fleming, C. J. Burrows, *Biophys. J.* **2018**, *114*, 1804.
[27] P. Školáková, D. Renčiuk, J. Palacký, D. Krafčík, Z. Dvořáková, I. Kejnovská, K. Bednářová, M. Vorlíčková, *Nucleic Acids Res.* **2019**, *47*, 2177.
[28] P. Školáková, M. Gajarský, J. Palacký, D. Šubert, D. Renčiuk, L. Trantírek, J.-L. Mergny, M. Vorlíčková, *Nucleic Acids Res.* **2023**, *51*, 2950. https://doi.org/10.1093/nar/gkad119
[29] J. M. Benevides, S. A. Overman, G. J. Thomas, *J Raman Spectrosc* **2005**, *36*, 279.
[30] T. Miura, G. J. Thomas, *Biochemistry* **1994**, *33*, 7848.
[31] T. Miura, J. M. Benevides, G. J. Thomas, *J. Mol. Biol.* **1995**, *248*, 233.
[32] T. Miura, G. J. Thomas, *Biochemistry* **1995**, *34*, 9645.
[33] L. Laporte, G. J. Thomas, *Biochemistry* **1998**, *37*, 1327.
[34] L. Laporte, G. J. Thomas, *J. Mol. Biol.* **1998**, *281*, 261.
[35] C. Krafft, J. M. Benevides, G. J. Thomas, *Nucleic Acids Res.* **2002**, *30*, 3981.
[36] J. Palacky, M. Vorlickova, I. Kejnovska, P. Mojzes, *Nucleic Acids Res.* **2013**, *41*, 1005.
[37] J. Palacky, P. Mojzes, I. Kejnovska, M. Vorlickova, *J Raman Spectrosc* **2020**, *51*, 301.
[38] R. M. Abu-Ghazalah, S. Rutledge, L. W. Y. Lau, D. N. Dubins, R. B. Macgregor, A. S. Helmy, *Biochemistry* **2012**, *51*, 7357.
[39] S. J. Friedman, A. C. Terentis, *J Raman Spectrosc* **2016**, *47*, 259.
[40] C. Y. Wei, G. Q. Jia, J. L. Yuan, Z. C. Feng, C. Li, *Biochemistry* **2006**, *45*, 6681.

[41] F. Bianchi, L. Comez, R. Biehl, F. D'Amico, A. Gessini, M. Longo, C. Masciovecchio, C. Petrillo, A. Radulescu, B. Rossi, F. Sacchetti, F. Sebastiani, N. Violini, A. Paciaroni, *Nucleic Acids Res.* **2018**, *46*, 11927.
[42] S. di Fonzo, C. Bottari, J. W. Brady, L. Tavagnacco, M. Caterino, L. Petraccone, J. Amato, C. Giancola, A. Cesaro, *Phys. Chem. Chem. Phys.* **2019**, *21*, 2093.
[43] L. Comez, F. Bianchi, V. Libera, M. Longo, C. Petrillo, F. Sacchetti, F. Sebastiani, F. D'Amico, B. Rossi, A. Gessini, C. Masciovecchio, H. Amenitsch, C. Sissi, A. Paciaroni, *Phys. Chem. Chem. Phys.* **2020**, *22*, 11583.
[44] S. di Fonzo, J. Amato, F. D'Aria, M. Caterino, F. D'Amico, A. Gessini, J. W. Brady, A. Cesaro, B. Pagano, C. Giancola, *Phys. Chem. Chem. Phys.* **2020**, *22*, 8128.
[45] V. Libera, F. Bianchi, B. Rossi, F. D'Amico, C. Masciovecchio, C. Petrillo, F. Sacchetti, A. Paciaroni, L. Comez, *Int. J. Mol. Sci.* **2022**, *23*, 13.
[46] F. D'Amico, R. Graziano, F. D'Aria, P. Russomanno, S. di Fonzo, J. Amato, B. Pagano, *Spectrochim. Acta A Mol. Biomol. Spectrosc.* **2023**, *300*, 122901.
[47] J. M. Benevides, C. Kang, G. J. Thomas, *Biochemistry* **1996**, *35*, 5747.
[48] J. Amato, N. Iaccarino, F. D'Aria, F. D'Amico, A. Randazzo, C. Giancola, A. Cesaro, S. di Fonzo, B. Pagano, *Phys. Chem. Chem. Phys.* **2022**, *24*, 7028.
[49] I. Kejnovska, D. Renciuk, J. Palacky, M. Vorlickova, in *G-Quadruplex Nucleic Acids: Methods and Protocols*, (Eds: D. Yang, C. Lin) Vol. 2035, Humana Press Inc, Totowa **2019** 25.
[50] J. Palacky, P. Mojzes, J. Bok, *J Raman Spectrosc* **2011**, *42*, 1528.
[51] L. Movileanu, J. M. Benevides, G. J. Thomas, *Nucleic Acids Res.* **2002**, *30*, 3767.
[52] F. D'Amico, M. Saito, F. Bencivenga, M. Marsi, A. Gessini, G. Camisasca, E. Principi, R. Cucini, S. di Fonzo, A. Battistoni, E. Giangrisostomi, C. Masciovecchio, *Nucl Instrum Meth Phys Res Sect Acc Spect Detect Assoc Equip* **2013**, *703*, 33.
[53] M. Ludwig, S. A. Asher, *Appl. Spectrosc.* **1988**, *42*, 1458.
[54] Z. M. Hong, S. A. Asher, *Appl. Spectrosc.* **2015**, *69*, 75.
[55] L. M. Uriarte, L. J. Bonales, J. Dubessy, A. Lobato, V. G. Baonza, M. Caceres, *Microchem. J.* **2018**, *139*, 134.
[56] M. Dracinsky, L. Benda, P. Bour, *Chem Phys Lett* **2011**, *512*, 54.
[57] E. R. Malinowski **2002**, 432.
[58] S. M. Reilly, R. K. Morgan, T. A. Brooks, R. M. Wadkins, *Biochemistry* **2015**, *54*, 1364.
[59] S. P. Gurung, C. Schwarz, J. P. Hall, C. J. Cardin, J. A. Brazier, *Chem. Commun.* **2015**, *51*, 5630.
[60] S. P. A. Fodor, R. P. Rava, T. R. Hays, T. G. Spiro, *J. Am. Chem. Soc.* **1985**, *107*, 1520.
[61] S. P. A. Fodor, T. G. Spiro, *J. Am. Chem. Soc.* **1986**, *108*, 3198.
[62] Z. Q. Wen, G. J. Thomas, *Biopolymers* **1998**, *45*, 247.
[63] J. Klener, J. Stepanek, *J Raman Spectrosc* **2021**, *52*, 678.
[64] D. Tsankov, M. Krasteva, V. Andrushchenko, J. H. van de Sande, H. Wieser, *Biophys. Chem.* **2006**, *119*, 1.
[65] A. Jirasek, H. G. Schulze, C. H. Hughesman, A. L. Creagh, C. A. Haynes, M. W. Blades, R. F. B. Turner, *J Raman Spectrosc* **2006**, *37*, 1368.
[66] M. Tsuboi, M. Komatsu, J. Hoshi, E. Kawashima, T. Sekine, Y. Ishido, M. P. Russell, J. M. Benevides, G. J. Thomas, *J. Am. Chem. Soc.* **1997**, *119*, 2025.
[67] X. M. Zhu, H. G. Wang, X. M. Zheng, D. L. Phillips, *J. Phys. Chem. B* **2008**, *112*, 15828.

SUPPORTING INFORMATION

Additional supporting information can be found online in the Supporting Information section at the end of this article.

How to cite this article: J. Palacký, P. Školáková, D. Renčiuk, P. Mojzeš, B. Rossi, F. Matroodi, M. Vorlíčková, *J Raman Spectrosc* **2024**, *55*(1), 43. https://doi.org/10.1002/jrs.6606